

Observation of Interfacial Antiferromagnetic Coupling between Magnetic Topological Insulator and Antiferromagnetic Insulator

Fei Wang^{1,2*}, Di Xiao^{1*}, Wei Yuan^{3,4*}, Jue Jiang¹, Yi-Fan Zhao¹, Ling Zhang¹, Yunyan Yao³, Baojuan Dong², Wei Liu², Zhidong Zhang², Chaoxing Liu¹, Jing Shi⁴, Wei Han^{3,5}, Moses H. W. Chan¹, Nitin Samarth¹, and Cui-Zu Chang¹

¹Department of Physics, Pennsylvania State University, University Park, Pennsylvania 16802, USA

²Shenyang National Laboratory for Materials Science, Institute of Metal Research, Chinese Academy of Sciences, Shenyang 110016, China

³International Center for Quantum Materials, School of Physics, Peking University, Beijing 100871, China

⁴Department of Physics, University of California, Riverside, California 92521, USA

⁵Collaborative Innovation Center of Quantum Matter, Beijing 100871, China

**These authors contributed equally to this work.*

Corresponding authors: cxc955@psu.edu (C.Z.C.).

Inducing magnetic orders in a topological insulator (TI) to break its time reversal symmetry has been predicted to reveal many exotic topological quantum phenomena. The manipulation of magnetic orders in a TI layer can play a key role in harnessing these quantum phenomena towards technological applications. Here we fabricated a thin magnetic TI film on an antiferromagnetic (AFM) insulator Cr₂O₃ layer

and found that the magnetic moments of the magnetic TI layer and the surface spins of the Cr₂O₃ layers favor interfacial AFM coupling. Field cooling studies show a crossover from negative to positive exchange bias clarifying the competition between the interfacial AFM coupling energy and the Zeeman energy in the AFM insulator layer. The interfacial exchange coupling also enhances the Curie temperature of the magnetic TI layer. The unique interfacial AFM alignment in magnetic TI on AFM insulator heterostructures opens a new route toward manipulating the interplay between topological states and magnetic orders in spin-engineered heterostructures, facilitating the exploration of proof-of-concept TI-based spintronic and electronic devices with multi-functionality and low power consumption.

Topological insulator (TI), a material in which the interior is insulating but the electrons can travel without resistance along its surface/edge conducting channels, has radically changed the research landscape of condensed matter physics and material science in the past decade [1,2]. The nontrivial Dirac surface/edge states of a TI are induced by the strong spin-orbit coupling of the material and thus protected by time-reversal symmetry (TRS) [3-6]. Breaking the TRS of a TI with a magnetic perturbation can lead to a variety of exotic quantum phenomena such as the quantum anomalous Hall (QAH) effect [7-9], topological magnetoelectric effect [8,10], and image magnetic monopole [11]. The QAH effect has been experimentally demonstrated in magnetically doped TI thin films, specifically Cr- and/or V-doped (Bi,Sb)₂Te₃ [12,13]. To date, the critical temperature of the QAH state (T_{QAH}) which we define as the temperature below which the quantized Hall resistance is realized, in magnetically doped TI films is still $\sim 1\text{K}$ [12-15]. A low T_{QAH} impedes both the exploration of

fundamental physics and meaningful technological applications based on this exotic phenomenon. A direct route to increase T_{QAH} is to increase the magnetic doping level in the TI film to enhance the Curie temperature (T_{C}). However, this process invariably degrades the quality of TI films and can even make it become trivial [16]. An alternative approach to induce the ferromagnetic (FM) order in TI but keep its nontrivial property is called for.

FM order can also be introduced into a TI layer through proximity to an FM insulator layer. By not introducing magnetic ions into the TI, the sample quality, in particular, the carrier mobility is expected to be much higher [17]. Experimental efforts along this line have demonstrated proximity induced interfacial magnetization in TIs with a few FM insulators, including EuS [18,19], GdN [20], BaFe₁₂O₁₉ [21], Cr₂Ge₂Te₆ [22] and ferrimagnet yttrium/thulium iron garnet (YIG/TIG) [23-26]. Since the magnetic proximity effect is a short-range magnetic exchange interaction, an antiferromagnetic (AFM) insulator layer with uncompensated surface spins could play the same role as FM insulators [27]. AFM insulators have a number of advantages compared with FM insulators, such as their insensitivity to perturbing magnetic fields, the high THz operating frequencies, and the negligible stray fields. These are attractive properties for spintronic applications [28-30]. Since the Néel temperature (T_{N}) of AFM insulator is usually well above the room temperature, it may be possible to induce a high Curie temperature (T_{C}) FM order in a TI. Recently, a transport cum neutron scattering experiment has found the interfacial spin texture modulation and the T_{C} enhancement in magnetically doped TI on AFM metal CrSb heterostructures [31]. In view of the metallic property of CrSb, it is not possible to single out the transport property of the TI layer from that of CrSb. Therefore, an insulating AFM substrate (i.e., AFM insulator) is a

better candidate to induce magnetic orders in the TI layer. We know of no study to date on such an experimental system.

In this *Letter*, we grew AFM insulator Cr_2O_3 layers with different thicknesses on heat-treated sapphire (0001) substrate to be followed with 4 quintuple layers (QL) magnetic TI $\text{Sb}_{1.8}\text{Cr}_{0.2}\text{Te}_3$ layer to form $\text{Sb}_{1.8}\text{Cr}_{0.2}\text{Te}_3/\text{Cr}_2\text{O}_3$ heterostructures. We demonstrated that when the thickness of the Cr_2O_3 layer (m) is ≤ 3 -unit cell (UC, 1UC ~ 1.36 nm), the anomalous Hall (AH) hysteresis loops of the magnetic TI layer, measured by systematically changing the magnitude of the magnetic field ($\mu_0 H_{\text{CF}}$) employed for field cooling, show a crossover from negative to positive shifts (i.e., exchange bias) along the magnetic field axis. This observation indicates an interfacial AFM coupling between the magnetic moments of the magnetic TI layers and the surface spins of the AFM Cr_2O_3 layer. The crossover of negative to positive exchange bias disappears for $m \geq 4$ UC because the T_{N} of the thicker Cr_2O_3 layer is higher than the T_{C} of the magnetic TI layer and this makes the surface spins of the AFM layer aligned randomly and smears out the appearance of the exchange bias. Upon further increase of the thickness of the Cr_2O_3 layer, the T_{C} of $\text{Sb}_{1.8}\text{Cr}_{0.2}\text{Te}_3$ layers is progressively enhanced from ~ 39 K without the Cr_2O_3 layer (see Supporting Materials) to ~ 50 K for Cr_2O_3 layer thicker than 14UC. The T_{C} enhancement also confirms the existence of the interfacial exchange coupling between magnetic TI and the Cr_2O_3 layers.

Bulk Cr_2O_3 is a well-known AFM insulator with a T_{N} of 307K [32], whose linear magnetoelectric property has been used in voltage-controlled spintronic devices [33-35]. The spins along the (0001) direction in the intralayer are FM aligned, while the spins of the adjacent layers are AFM coupled (**Fig. 1a**). It is known that the T_{C} (T_{N}) of the FM (AFM)

films due to the finite size effect is usually lower than its bulk value [36,37]. Therefore, the T_N of AFM Cr_2O_3 films can be controlled by varying m . The Cr_2O_3 layers with different m (from 1 to 35 UC) were deposited at 500°C by pulsed laser deposition (PLD) on heat-treated sapphire (0001) substrates [38,39]. The growth process was monitored by *in-situ* reflection high-energy electron diffraction (RHEED). The sharp and streaky “ 1×1 ” patterns indicate highly-ordered Cr_2O_3 films with atomically flat surfaces (**Fig. S1**). The high quality of the Cr_2O_3 films is also confirmed by atomic force microscopy and high-resolution X-ray diffraction (HR-XRD) measurements (**Figs. S2 and S3**).

The growth of the 4 QL $\text{Sb}_{1.8}\text{Cr}_{0.2}\text{Te}_3$ films on AFM Cr_2O_3 layers was carried out in a molecular beam epitaxy (MBE) chamber with a base pressure of 2×10^{-10} mbar. During the growth of the magnetic TI film, the Cr_2O_3 /sapphire substrate was maintained at $\sim 240^\circ\text{C}$. This low MBE growth temperature inhibits the diffusion of the Cr atoms into the Cr-doped Sb_2Te_3 layer. The high quality of the 4QL $\text{Sb}_{1.8}\text{Cr}_{0.2}\text{Te}_3$ is confirmed by sharp “ 1×1 ” RHEED patterns, the smooth atomic force microscopy image that shows a roughness of ~ 0.9 nm over $5\mu\text{m} \times 5\mu\text{m}$ area and the sharp $(00n)$ peaks in the HR-XRD spectroscopy (**Figs. S4 to S6**). To avoid possible contamination, a 10 nm thick Te layer was deposited at room temperature on the magnetic TI film prior to the removal of the heterostructure samples from the MBE chamber for *ex-situ* measurements.

Figure 1b shows the cross-sectional scanning transmission electron microscopy (STEM) image of the 10nm Te capped 4QL $\text{Sb}_{1.8}\text{Cr}_{0.2}\text{Te}_3$ /35UC Cr_2O_3 heterostructure grown on a sapphire substrate and the corresponding energy dispersive spectroscopy (EDS) mappings of Al, Cr, Sb, and Te. Al and Cr are found residing at the sapphire substrate and

Cr₂O₃ layers, respectively, while Sb and Te are found in the Cr-doped TI and Te capping layers. The absence of the Cr signal in Cr-doped Sb₂Te₃ is due to the low concentration of Cr in the TI layer. The trace Sb signal showing in the Te capping layer is a result of their neighboring peak positions in the X-ray spectrum. More TEM and EDS results on other two heterostructures (7 QL Sb_{1.8}Cr_{0.2}Te₃/3UC Cr₂O₃ and 4QL Sb_{1.8}Cr_{0.2}Te₃/14UC Cr₂O₃) are shown in Supporting Materials (**Fig. S7**).

The 10nm Te capped 4QL Sb_{1.8}Cr_{0.2}Te₃/*m* UC Cr₂O₃ heterostructure samples were scratched into a Hall bar geometry using a computer-controlled probe station [10]. Transport studies were carried out in a Physical Property Measurement System (Quantum Design, 2 K, 9 T) with an external magnetic field perpendicular to the film. The excitation current is 1 μA. All samples were field cooled from 320K, which is above T_N of bulk Cr₂O₃ (~307K) [32], at different specific external magnetic fields $\mu_0 H_{CF}$ to the target measurement temperatures. The field cooling process eliminates any possible spontaneous and random alignments of the AFM order in the Cr₂O₃ layer. **Figure 2a** shows the magnetic field ($\mu_0 H$) dependence of the Hall resistance (ρ_{yx}) at 2K of the 4QL Sb_{1.8}Cr_{0.2}Te₃/3UC Cr₂O₃ heterostructure field cooled at $\mu_0 H_{CF} = 0.05, 0.3, 0.8, 2$ and 7T. The blue (red) curves correspond to ρ_{yx} measured while sweeping $\mu_0 H$ downward from 0.2T to -0.2T (upward from -0.2T to 0.2T). The small $\mu_0 H$ sweep range is chosen to make sure the spin orders of the AFM layers induced by the field cooling procedure are preserved. The nearly square ρ_{yx} hysteresis loops confirm a well-defined FM order with perpendicular magnetic anisotropy in these films [12,40]. The ρ_{yx} loop for the sample prepared at $\mu_0 H_{CF} = 0.05$ T shows a negative exchange bias, i.e., the left coercive field $|\mu_0 H_{CL}|$ is larger than the right coercive field $\mu_0 H_{CR}$ thus indicating the presence

of a unidirectional magnetic exchange anisotropy across the $\text{Sb}_{1.8}\text{Cr}_{0.2}\text{Te}_3/\text{Cr}_2\text{O}_3$ interface. The $\mu_0 H_{\text{CF}} = 0.3\text{T}$ loop still shows the negative exchange bias, but the magnitude of the shift is reduced. The $\mu_0 H_{\text{CF}} = 0.8\text{T}$ loop is nearly symmetric, aka, $|\mu_0 H_{\text{cL}}| = \mu_0 H_{\text{cR}}$. Upon further increase of $\mu_0 H_{\text{CF}}$ to 2T, the negative exchange bias (i.e., $|\mu_0 H_{\text{cL}}| > \mu_0 H_{\text{cR}}$) is replaced by positive exchange bias (i.e., $|\mu_0 H_{\text{cL}}| < \mu_0 H_{\text{cR}}$). The positive exchange bias becomes more pronounced if the sample is cooled under $\mu_0 H_{\text{CF}} = 7\text{T}$. The observation of a crossover from negative to positive exchange bias indicates that opposite AFM domain states in the Cr_2O_3 layer were established under different $\mu_0 H_{\text{CF}}$.

The Hall traces of the 4QL $\text{Sb}_{1.8}\text{Cr}_{0.2}\text{Te}_3/2\text{UC Cr}_2\text{O}_3$ and 4QL $\text{Sb}_{1.8}\text{Cr}_{0.2}\text{Te}_3/1\text{UC Cr}_2\text{O}_3$ are shown respectively in **Figs. 2b** and **2c**. These two samples also display negative exchange bias under low $\mu_0 H_{\text{CF}}$ and positive exchange bias under high $\mu_0 H_{\text{CF}}$. **Figures 2a** to **2c** show that the $\mu_0 H_{\text{CF}}$ at which a symmetric ρ_{yx} loop is found monotonically decreases with decreasing thickness of the Cr_2O_3 layers. The magnitude of the exchange bias field ($\mu_0 H_{\text{E}}$) is defined as $(\mu_0 H_{\text{cR}} - |\mu_0 H_{\text{cL}}|)/2$. The $\mu_0 H_{\text{E}}$ as a function of $\mu_0 H_{\text{CF}}$ at $T=2\text{K}$ for the 4 QL $\text{Sb}_{1.8}\text{Cr}_{0.2}\text{Te}_3/m$ UC Cr_2O_3 heterostructures ($m=1\sim 4$) are summarized in **Fig. 2d**. We note that for $m \leq 3$ UC, the $\mu_0 H_{\text{E}}$ changes from a negative value through zero to a positive value when the $\mu_0 H_{\text{CF}}$ is discretely increased from 0.05T to 7T. The critical $\mu_0 H_{\text{CF}}$ with $\mu_0 H_{\text{E}} = 0$ is labeled as $\mu_0 H_{\text{CF}}^0$. The $\mu_0 H_{\text{CF}}^0$ are 0.8T, 0.7T and 0.3T for 3UC, 2UC, and 1UC Cr_2O_3 layers, respectively (Inset of **Fig. 2d**). However, for $m = 4$ UC, the ρ_{yx} loop is always symmetric, i.e., showing a negligible shift under all $\mu_0 H_{\text{CF}}$, indicating the suppression of an exchange bias effect (**Fig. 2d** and **Fig. S9**).

Magnetic hysteresis loop shifts as a result of the interfacial exchange interaction have

been observed in many systems with FM-AFM interfaces [41]. The AFM layer usually plays the role of a pinning layer, whose alignment direction determines the shift direction of the hysteresis loop. In most systems, the shift of the hysteresis loop is along the direction opposite to $\mu_0 H_{CF}$, i.e., showing negative exchange bias, which is an evidence for the interfacial FM coupling [41]. In our Cr-doped Sb_2Te_3 on Cr_2O_3 heterostructures, we observed the crossover of the negative to positive exchange bias by systematically increasing $\mu_0 H_{CF}$. The observation of the positive exchange bias under high $\mu_0 H_{CF}$ is a necessary condition for the interfacial AFM coupling between the magnetic moments of the FM layer and the surface spins of the AFM layer [41-44]. More details will be shown below.

Next, we focus on the study of the evolution of positive $\mu_0 H_E$ of 4QL $\text{Sb}_{1.8}\text{Cr}_{0.2}\text{Te}_3$ on Cr_2O_3 of 3, 2 and 1UC field-cooled with $\mu_0 H_{CF} = 7\text{T}$. The ρ_{yx} hysteresis loops of these heterostructures at temperatures from 2 to 40K are shown respectively in **Figs. 3a** to **3c**. These loops show that $\mu_0 H_{cR}$, $|\mu_0 H_{cL}|$, and the positive $\mu_0 H_E$, all monotonically decrease with increasing temperature. **Figure 3d** shows $\mu_0 H_E$ as a function of temperature for these heterostructures. The blocking temperature T_B , i.e., the temperature above which $\mu_0 H_E$ vanishes, increases with increasing m of the Cr_2O_3 layers. The T_B s for the heterostructures with 1UC, 2UC, and 3UC Cr_2O_3 layers are 15K, 25K, and 35K, respectively. The higher T_B in the heterostructures with thicker Cr_2O_3 layers suggests the T_N is higher in thicker Cr_2O_3 layers.

To achieve the exchange bias effect in the systems with the FM-AFM interface, the T_N of the AFM layer must be lower than the T_C of the FM layer. Therefore, for $m \leq 3\text{UC}$, the T_N of Cr_2O_3 layer must be lower than the $T_C \sim 38\text{K}$ of 4QL $\text{Sb}_{1.8}\text{Cr}_{0.2}\text{Te}_3$ (**Fig. S13**). We now

explain why the observation of the crossover from the negative to positive exchange bias demonstrates the magnetic moments of the Cr-doped Sb_2Te_3 and Cr_2O_3 layers are AFM coupled. Since $T_C \geq T_N$, during the cooling of the samples under a positive $\mu_0 H_{CF}$, the temperature first arrives at $T=T_C$, the magnetic moments of the 4QL $\text{Sb}_{1.8}\text{Cr}_{0.2}\text{Te}_3$ layer are consequently aligned upwards as shown in **Figs. 4a** and **4b**. With further cooling to $T = T_N$, the AFM order is formed in Cr_2O_3 layers. If the AFM and FM layers favor the interfacial AFM coupling, the spins of the aligned $\text{Sb}_{1.8}\text{Cr}_{0.2}\text{Te}_3$ layer exert an effective field to force the surface spins of the Cr_2O_3 layer to be oppositely aligned, i.e., pointing downwards. The AFM coupling energy between the AFM and FM layers is $J_E S_{AFM} S_{FM}$, where J_E is the exchange coupling strength between the surface spins of Cr_2O_3 (S_{AFM}) and $\text{Sb}_{1.8}\text{Cr}_{0.2}\text{Te}_3$ (S_{MTI}) layers. In addition, the Zeeman energy in the AFM layer under the external magnetic field $\mu_0 H_{CF}$ is $\mu_0 H_{CF} M_{AFM}$, where M_{AFM} is the surface magnetization of the AFM Cr_2O_3 layer. This Zeeman energy forces the surface spins of the Cr_2O_3 layer to be aligned along the direction of the external magnetic field [42,44]. The alignment between AFM and FM layers is determined by the competition between the AFM coupling energy $J_E S_{AFM} S_{FM}$ and the Zeeman energy in the AFM layer $\mu_0 H_{CF} M_{AFM}$.

When the sample is field-cooled under a low $\mu_0 H_{CF}$, $\mu_0 H_{CF} M_{AFM} < J_E S_{AFM} S_{FM}$ (**Fig. 4a**), the AFM coupling energy $J_E S_{AFM} S_{FM}$ is then dominant and, as a consequence, the positive magnetization of the Cr-doped Sb_2Te_3 will force the top surface spins of the Cr_2O_3 layer to point downwards. With a high $\mu_0 H_{CF}$, $\mu_0 H_{CF} M_{AFM} > J_E S_{AFM} S_{FM}$ (**Fig. 4b**), the Zeeman energy in Cr_2O_3 layer $\mu_0 H_{CF} M_{AFM}$ is dominant and makes the top surface spins of the Cr_2O_3 layer to point upwards. To compensate for the AFM coupling, the orientation of the

surface spins in the Cr₂O₃ layer will be slightly tilted. Since the magnetic field sweep range $\pm 0.2\text{T}$ is much lower than the magnetic field at which the spin-flop transition, reported to occur at a few Teslas [39,45], the adjacent magnetic layers in the Cr₂O₃ layer are still AFM ordered but are slightly tilted (**Fig. 4b**). With a critical value of $\mu_0 H_{CF}$ (i.e., $\mu_0 H_{CF}^0$), $\mu_0 H_{CF}^0 = M_{AFM} = J_E S_{AFM} S_{FM}$, the Cr₂O₃ layer is in a randomly distributed multi-domain state, and thus $\mu_0 H_E = 0$, and gives rise to the symmetric hysteresis loop. $\mu_0 H_{CF}^0$ increases with m as a result of the J_E enhancement, which is induced by the higher T_N in thicker Cr₂O₃ layers [44].

The surface spin configuration of the Cr₂O₃ layer at low temperature is locked by its AFM magnetic structure during the field cooling process. When the external $\mu_0 H$ is swept in the $\pm 0.2\text{T}$ range the FM spins of the 4QL Sb_{1.8}Cr_{0.2}Te₃ layer with a $\mu_0 H_c$ of $\sim 0.1\text{T}$ can be switched by the external magnetic field while the AFM spins of the Cr₂O₃ layer are unchanged [39,45]. The existence of the AFM coupling energy $J_E S_{AFM} S_{FM}$ across Cr-doped Sb₂Te₃ and Cr₂O₃ interface will cause the shift of the FM hysteresis loop of the 4QL Sb_{1.8}Cr_{0.2}Te₃ layer. For samples field cooled with a low $\mu_0 H_{CF}$, the top surface spins of the Cr₂O₃ layer are locked downwards when $\mu_0 H$ is swept at $T=2\text{K}$ and the magnetic moments of the 4QL Sb_{1.8}Cr_{0.2}Te₃ layer are pointing upwards for $\mu_0 H = 0.2\text{T}$ (Step I in **Fig. 4c**). When $\mu_0 H$ is swept downward, near the left coercive field $\mu_0 H_{cL}$, the upward magnetic domains of the 4QL Sb_{1.8}Cr_{0.2}Te₃ layer is reversed. Due to the interfacial AFM coupling, the spins of Sb_{1.8}Cr_{0.2}Te₃ are energetically more favorable to point upwards to retain the antiparallel alignment. Therefore, to overcome the interfacial AFM coupling energy, a magnetic field $\mu_0 H$ larger than $\mu_0 H_c$ is needed to reverse the magnetic domains from upwards to downward, i.e., $|\mu_0 H_{cL}| > \mu_0 H_c$ (Step II in **Fig. 4c**). When $\mu_0 H$ is swept back from -0.2T , the presence of the

interfacial AFM coupling helps the magnetization reversal of 4QL $\text{Sb}_{1.8}\text{Cr}_{0.2}\text{Te}_3$ layer from parallel to antiparallel alignments, so the right coercive field $\mu_0 H_{cR} < \mu_0 H_c$ (Step IV in **Fig. 4c**). This explains why negative exchange bias, i.e., $|\mu_0 H_{cL}| > \mu_0 H_{cR}$, is observed under a low $\mu_0 H_{CF}$.

When the sample is field-cooled under a high $\mu_0 H_{CF}$, the magnetic moments at $\mu_0 H = 0.2\text{T}$ of the Cr-doped Sb_2Te_3 are still pointing upwards, but the top surface spins of the Cr_2O_3 layer are also pointing upwards but slightly tilted (Step I in **Fig. 4d**). When $\mu_0 H$ is swept downward, the existence of the AFM coupling will favor the magnetization reversal of 4QL $\text{Sb}_{1.8}\text{Cr}_{0.2}\text{Te}_3$ layer from upwards to downwards, so $|\mu_0 H_{cL}| < \mu_0 H_c$ (Step II in **Fig. 4d**). When $\mu_0 H$ is swept back from -0.2T , the interfacial AFM coupling will impede the magnetization reversal of 4QL $\text{Sb}_{1.8}\text{Cr}_{0.2}\text{Te}_3$ layer from downwards to upwards, so $\mu_0 H_{cR} > \mu_0 H_c$. This corresponds to the positive exchange bias, i.e., $|\mu_0 H_{cL}| < \mu_0 H_{cR}$, observed for the samples field cooled with a high $\mu_0 H_{CF}$.

We have also systematically studied the T_C of the 4QL $\text{Sb}_{1.8}\text{Cr}_{0.2}\text{Te}_3$ layer for $m \geq 4$. The T_C of 4QL $\text{Sb}_{1.8}\text{Cr}_{0.2}\text{Te}_3$ layer in all heterostructures was determined by the Arrott-plots (**Fig. S11**) [46]. The m dependence of T_C is summarized in **Fig. S12**. For $m \leq 4\text{UC}$, T_C is $\sim 39\text{K}$, consistent with the T_C of 4QL $\text{Sb}_{1.8}\text{Cr}_{0.2}\text{Te}_3$ film grown on the nonmagnetic $\text{SrTiO}_3(111)$ substrate (**Fig. S13**). For $m \geq 5\text{UC}$, the T_C starts to increase and saturates near 50K for $m \geq 14\text{UC}$. The T_C enhancement of 4QL $\text{Sb}_{1.8}\text{Cr}_{0.2}\text{Te}_3$ grown on the thicker Cr_2O_3 films further demonstrate the existence of the interfacial exchange coupling.

To summarize, we demonstrated the tuning of the exchange bias in a given magnetic TI on AFM insulator heterostructure from negative to positive values by field cooling with

different $\mu_0 H_{CF}$. This is made possible by the interfacial AFM coupling between the FM aligned spins of the magnetic TI layer and the surface spins of the AFM insulator. This efficient tuning of the exchange bias provides a new route to effectively manipulate the magnetic spins of the TI layer. Our findings, when combined with the linear magnetoelectric effect of Cr_2O_3 [33-35], could facilitate the development of proof-of-concept electric field-controlled TI-based energy-efficient spintronic devices.

Acknowledgments

The authors would like to thank B. H. Yan and X. D. Xu for the helpful discussions. F. W., Y. Z. and C. Z. C. acknowledge the support from ARO Young Investigator Program Award (W911NF1810198) and the Alfred P. Sloan Research Fellowship. D. X. and N. S. acknowledge the support from the Penn State Two-Dimensional Crystal Consortium-Materials Innovation Platform (2DCC-MIP) under NSF grant DMR-1539916 and the Office of Naval Research (N00014-15-1-2370). C. X. L. acknowledges the support from the Office of Naval Research (N00014-15-1-2675). F. W., W. L., and Z. D. Z. acknowledge the support from the State Key Program of Research and Development of China (2017YFA0206302), the National Natural Science Foundation of China (NSFC) (51590883, 51331006 and 51771198) and the Key Research Program of Chinese Academy of Sciences (KJZD-EW-M05-3). J. S. acknowledges the support from DOE grant (DE-FG02-07ER46351). W. H. acknowledges the support from the National Basic Research Programs of China (2015CB921104) and the National Natural Science Foundation of China (NSFC) (11574006). Support for the electrical transport measurements and data analysis is provided by the DOE grant (DE-SC0019064).

Figures and figure captions:

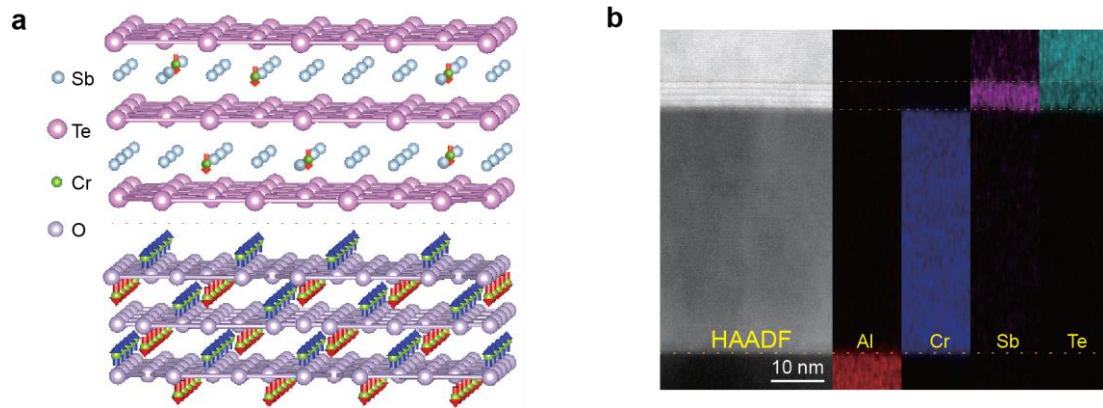


Figure 1| The magnetic TI Cr-doped Sb₂Te₃/AFM Cr₂O₃ heterostructure. (a) Schematic atomic structure of the Cr-doped Sb₂Te₃/Cr₂O₃ heterostructure. The magnetic moments of Cr-doped Sb₂Te₃ and the surface spins of the Cr₂O₃ layer are AFM aligned. (b) STEM image of the Te layer-capped 4 QL Sb_{1.8}Cr_{0.2}Te₃/35UC Cr₂O₃ heterostructure grown on a sapphire substrate, accompanied by an EDS map of Al, Cr, Sb, and Te of the sample.

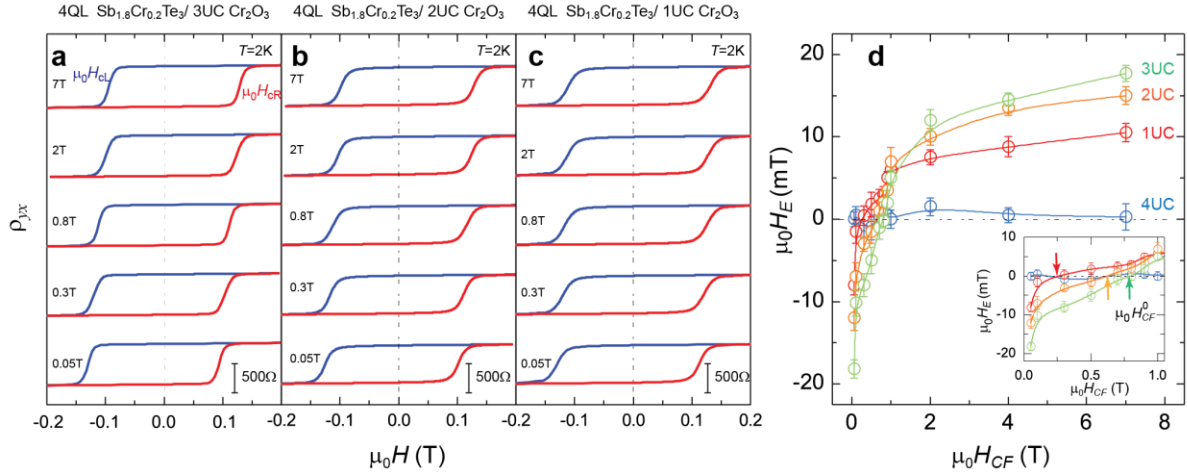


Figure 2| AFM interfacial coupling between Cr-doped Sb_2Te_3 and Cr_2O_3 layers as revealed by the observation of crossover from negative to positive exchange bias. (a, b, c) The Hall resistance ρ_{yx} at $T = 2\text{K}$ of 4 QL $\text{Sb}_{1.8}\text{Cr}_{0.2}\text{Te}_3$ layer grown on 3 UC (a), 2 UC (b), 1 UC (c) Cr_2O_3 layers field cooled with $\mu_0 H_{\text{CF}} = 0.05, 0.3, 0.8, 2,$ and 7T . (d) The exchange bias $\mu_0 H_E$ as a function of $\mu_0 H_{\text{CF}}$ at $T = 2\text{K}$ for 4 QL $\text{Sb}_{1.8}\text{Cr}_{0.2}\text{Te}_3$ grown on 1~4 UC Cr_2O_3 layers. Note that $\mu_0 H_E$ is negligible in the 4 QL $\text{Sb}_{1.8}\text{Cr}_{0.2}\text{Te}_3/4$ UC Cr_2O_3 heterostructure since the T_N of 4 UC Cr_2O_3 layer is higher than T_C of 4 QL $\text{Sb}_{1.8}\text{Cr}_{0.2}\text{Te}_3$ layer. The error bars reflect the standard deviations of the left and right coercive fields $\mu_0 H_{\text{CL}}$ and $\mu_0 H_{\text{CR}}$ used in the $\mu_0 H_E$ calculations. The inset shows the zoomed-in low $\mu_0 H_{\text{CF}}$ region. The horizontal intercepts denoted by the arrows become larger in heterostructures with the thicker Cr_2O_3 layer.

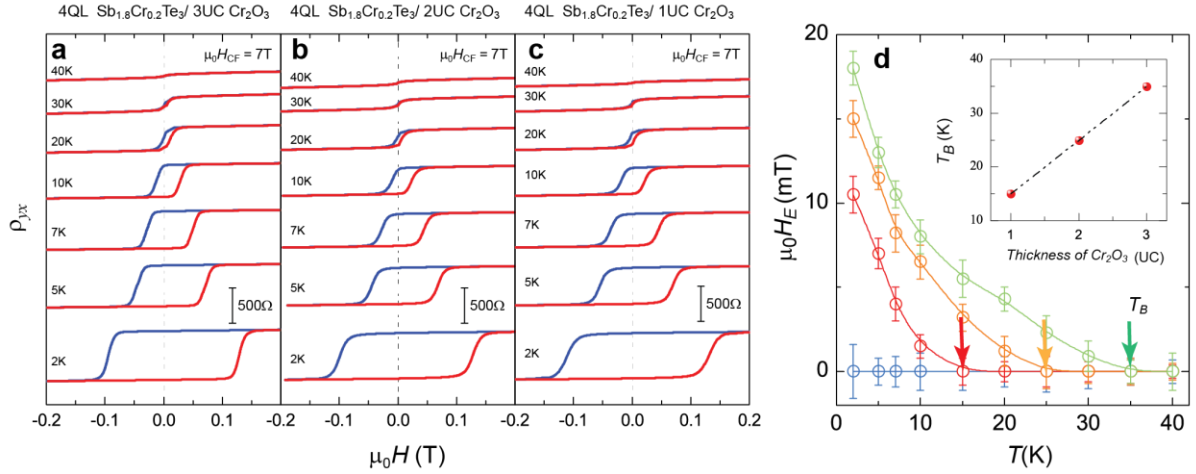


Figure 3| Temperature dependence of the positive exchange bias in Cr-doped $\text{Sb}_2\text{Te}_3/\text{Cr}_2\text{O}_3$ heterostructures field cooled at $\mu_0 H_{CF}=7\text{T}$. (a, b, c) The Hall resistance ρ_{yx} at varying temperatures of 4 QL $\text{Sb}_{1.8}\text{Cr}_{0.2}\text{Te}_3$ layer on 3 UC (a), 2 UC (b), 1 UC (c) Cr_2O_3 layers. (d) Temperature dependence of the exchange bias $\mu_0 H_E$ in 4 QL $\text{Sb}_{1.8}\text{Cr}_{0.2}\text{Te}_3$ grown on 1~4 UC Cr_2O_3 heterostructures. The blocking temperature T_B , at which $\mu_0 H_E=0$, increases with increasing thickness of the Cr_2O_3 layer. The magnitude of the error bars reflects the standard deviations of the $\mu_0 H_{cL}$ and $\mu_0 H_{cR}$ used in calculating $\mu_0 H_E$. Inset shows T_B as a function of the thickness of the Cr_2O_3 layer in the heterostructures.

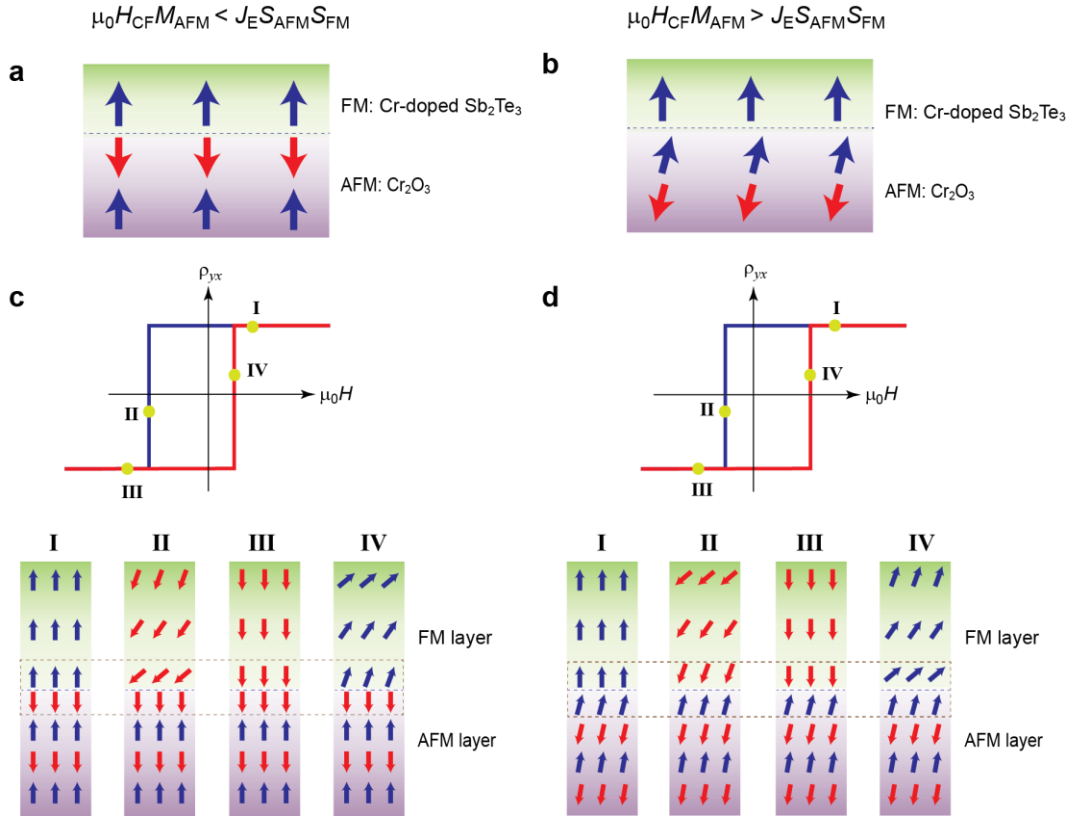


Figure 4 | A schematic of the model of interfacial AFM coupling between Cr-doped Sb_2Te_3 and Cr_2O_3 layers. (a, b) The orientations of the magnetic moments in the Cr-doped Sb_2Te_3 and Cr_2O_3 layers field cooled under low (a) and high (b) $\mu_0 H_{CF}$. When the heterostructure is field cooled under a low $\mu_0 H_{CF}$ ($\mu_0 H_{CF} M_{AFM} < J_E S_{AFM} S_{FM}$), the spins of the Cr-doped TI and Cr_2O_3 layers are AFM aligned. For a high $\mu_0 H_{CF}$ ($\mu_0 H_{CF} M_{AFM} > J_E S_{AFM} S_{FM}$), the spins of the Cr-doped TI and Cr_2O_3 layers are forced to be FM aligned. (c) Negative exchange bias and the spin switching process of the Cr-doped TI layer prepared with a low $\mu_0 H_{CF}$. (d) Positive exchange bias and the spin switching process of the Cr-doped TI layer prepared with a high $\mu_0 H_{CF}$.

References:

- [1] M. Z. Hasan and C. L. Kane, *Rev. Mod. Phys.* **82**, 3045 (2010).
- [2] X. L. Qi and S. C. Zhang, *Rev. Mod. Phys.* **83**, 1057 (2011).
- [3] B. A. Bernevig, T. L. Hughes, and S. C. Zhang, *Science* **314**, 1757 (2006).
- [4] M. Konig, S. Wiedmann, C. Brune, A. Roth, H. Buhmann, L. W. Molenkamp, X. L. Qi, and S. C. Zhang, *Science* **318**, 766 (2007).
- [5] H. J. Zhang, C. X. Liu, X. L. Qi, X. Dai, Z. Fang, and S. C. Zhang, *Nat. Phys.* **5**, 438 (2009).
- [6] D. Hsieh, Y. Xia, D. Qian, L. Wray, F. Meier, J. H. Dil, J. Osterwalder, L. Patthey, A. V. Fedorov, H. Lin, A. Bansil, D. Grauer, Y. S. Hor, R. J. Cava, and M. Z. Hasan, *Phys. Rev. Lett.* **103**, 146401 (2009).
- [7] F. D. M. Haldane, *Phys. Rev. Lett.* **61**, 2015 (1988).
- [8] X. L. Qi, T. L. Hughes, and S. C. Zhang, *Phys. Rev. B* **78**, 195424 (2008).
- [9] R. Yu, W. Zhang, H. J. Zhang, S. C. Zhang, X. Dai, and Z. Fang, *Science* **329**, 61 (2010).
- [10] D. Xiao, J. Jiang, J. H. Shin, W. B. Wang, F. Wang, Y. F. Zhao, C. X. Liu, W. D. Wu, M. H. W. Chan, N. Samarth, and C. Z. Chang, *Phys. Rev. Lett.* **120**, 056801 (2018).
- [11] X. L. Qi, R. D. Li, J. D. Zang, and S. C. Zhang, *Science* **323**, 1184 (2009).
- [12] C. Z. Chang, J. S. Zhang, X. Feng, J. Shen, Z. C. Zhang, M. H. Guo, K. Li, Y. B. Ou, P. Wei, L. L. Wang, Z. Q. Ji, Y. Feng, S. H. Ji, X. Chen, J. F. Jia, X. Dai, Z. Fang, S. C. Zhang, K. He, Y. Y. Wang, L. Lu, X. C. Ma, and Q. K. Xue, *Science* **340**, 167 (2013).
- [13] C. Z. Chang, W. W. Zhao, D. Y. Kim, H. J. Zhang, B. A. Assaf, D. Heiman, S. C. Zhang, C. X. Liu, M. H. W. Chan, and J. S. Moodera, *Nat. Mater.* **14**, 473 (2015).
- [14] M. Mogi, R. Yoshimi, A. Tsukazaki, K. Yasuda, Y. Kozuka, K. S. Takahashi, M. Kawasaki, and Y. Tokura, *Appl. Phys. Lett.* **107**, 182401 (2015).
- [15] Y. Ou, C. Liu, G. Jiang, Y. Feng, D. Zhao, W. Wu, X. X. Wang, W. Li, C. Song, L. L. Wang, W. Wang, W. Wu, Y. Wang, K. He, X. C. Ma, and Q. K. Xue, *Adv. Mater.* **30**, 1703062 (2017).
- [16] J. S. Zhang, C. Z. Chang, P. Z. Tang, Z. C. Zhang, X. Feng, K. Li, L. L. Wang, X. Chen, C. X. Liu, W. H. Duan, K. He, Q. K. Xue, X. C. Ma, and Y. Y. Wang, *Science* **339**, 1582 (2013).
- [17] C. Z. Chang, P. Wei, and J. S. Moodera, *MRS Bull.* **39**, 867 (2014).
- [18] P. Wei, F. Katmis, B. A. Assaf, H. Steinberg, P. Jarillo-Herrero, D. Heiman, and J. S. Moodera, *Phys. Rev. Lett.* **110**, 186807 (2013).
- [19] F. Katmis, V. Lauter, F. S. Nogueira, B. A. Assaf, M. E. Jamer, P. Wei, B. Satpati, J. W. Freeland, I. Eremin, D. Heiman, P. Jarillo-Herrero, and J. S. Moodera, *Nature* **533**, 513 (2016).
- [20] A. Kandala, A. Richardella, D. W. Rench, D. M. Zhang, T. C. Flanagan, and N. Samarth, *Appl. Phys. Lett.* **103**, 202409 (2013).
- [21] W. M. Yang, S. O. Yang, Q. H. Zhang, Y. Xu, S. P. Shen, J. Liao, J. Teng, C. W. Nan, L. Gu, Y. Sun, K. H. Wu, and Y. Q. Li, *Appl. Phys. Lett.* **105**, 092411 (2014).
- [22] L. D. Alegria, H. Ji, N. Yao, J. J. Clarke, R. J. Cava, and J. R. Petta, *Appl. Phys. Lett.* **105**, 053512 (2014).
- [23] H. L. Wang, J. Kally, J. S. Lee, T. Liu, H. C. Chang, D. R. Hickey, K. A. Mkhoyan, M. Z. Wu, A. Richardella, and N. Samarth, *Phys. Rev. Lett.* **117**, 076601 (2016).
- [24] M. R. Lang, M. Montazeri, M. C. Onbasli, X. F. Kou, Y. B. Fan, P. Upadhyaya, K. Y. Yao, F. Liu, Y. Jiang, W. J. Jiang, K. L. Wong, G. Q. Yu, J. S. Tang, T. X. Nie, L. He, R. N. Schwartz, Y. Wang, C. A. Ross, and K. L. Wang, *Nano Lett.* **14**, 3459 (2014).

- [25] Z. L. Jiang, C. Z. Chang, C. Tang, P. Wei, J. S. Moodera, and J. Shi, *Nano Lett.* **15**, 5835 (2015).
- [26] C. Tang, C. Z. Chang, G. Zhao, Y. Liu, Z. Jiang, C.-x. Liu, M. R. McCartney, D. J. Smith, T. Chen, J. S. Moodera, and J. Shi, *Sci. Adv.* **3**, e1700307 (2017).
- [27] W. D. Luo and X. L. Qi, *Phys. Rev. B* **87**, 085431 (2013).
- [28] V. Baltz, A. Manchon, M. Tsoi, T. Moriyama, T. Ono, and Y. Tserkovnyak, *Rev. Mod. Phys.* **90**, 015005 (2018).
- [29] L. Smejkal, Y. Mokrousov, B. H. Yan, and A. H. MacDonald, *Nat. Phys.* **14**, 242 (2018).
- [30] T. Jungwirth, X. Marti, P. Wadley, and J. Wunderlich, *Nat. Nanotechnol.* **11**, 231 (2016).
- [31] Q. L. He, X. F. Kou, A. J. Grutter, G. Yin, L. Pan, X. Y. Che, Y. X. Liu, T. X. Nie, B. Zhang, S. M. Disseler, B. J. Kirby, W. Ratcliff, Q. M. Shao, K. Murata, X. D. Zhu, G. Q. Yu, Y. B. Fan, M. Montazeri, X. D. Han, J. A. Borchers, and K. L. Wang, *Nat. Mater.* **16**, 94 (2017).
- [32] T. R. Mcguire, E. J. Scott, and F. H. Grannis, *Phys. Rev.* **102**, 1000 (1956).
- [33] X. He, Y. Wang, N. Wu, A. N. Caruso, E. Vescovo, K. D. Belashchenko, P. A. Dowben, and C. Binek, *Nat. Mater.* **9**, 579 (2010).
- [34] P. Borisov, A. Hochstrat, X. Chen, W. Kleemann, and C. Binek, *Phys. Rev. Lett.* **94**, 117203 (2005).
- [35] M. Fiebig, *J. Phys. D Appl. Phys.* **38**, R123 (2005).
- [36] K. Lenz, S. Zander, and W. Kuch, *Phys. Rev. Lett.* **98**, 237201 (2007).
- [37] T. Ambrose and C. L. Chien, *Phys. Rev. Lett.* **76**, 1743 (1996).
- [38] W. Yuan, T. Y. Wang, T. Su, Q. Song, W. Y. Xing, Y. Y. Chen, and W. Han, *J. Magn. Magn. Mater.* **422**, 397 (2017).
- [39] W. Yuan, Q. Zhu, T. Su, Y. Y. Yao, W. Y. Xing, Y. Y. Chen, Y. Ma, X. Lin, J. Shi, R. Shindou, X. C. Xie, and W. Han, *Sci. Adv.* **4**, eaat1098 (2018).
- [40] C. Z. Chang, J. S. Zhang, M. H. Liu, Z. C. Zhang, X. Feng, K. Li, L. L. Wang, X. Chen, X. Dai, Z. Fang, X. L. Qi, S. C. Zhang, Y. Y. Wang, K. He, X. C. Ma, and Q. K. Xue, *Adv. Mater.* **25**, 1065 (2013).
- [41] J. Nogues and I. K. Schuller, *J Magn Magn Mater* **192**, 203 (1999).
- [42] J. Nogues, D. Lederman, T. J. Moran, and I. K. Schuller, *Phys. Rev. Lett.* **76**, 4624 (1996).
- [43] J. Nogues, C. Leighton, and I. K. Schuller, *Phys. Rev. B* **61**, 1315 (2000).
- [44] D. Z. Yang, J. Du, L. Sun, X. S. Wu, X. X. Zhang, and S. M. Zhou, *Phys. Rev. B* **71**, 144417 (2005).
- [45] S. Seki, T. Ideue, M. Kubota, Y. Kozuka, R. Takagi, M. Nakamura, Y. Kaneko, M. Kawasaki, and Y. Tokura, *Phys. Rev. Lett.* **115**, 266601 (2015).
- [46] A. Arrott, *Phys. Rev.* **108**, 1394 (1957).